Journal of Solid State Chemistry **149,** 370–377 (2000)
doi:10.1006/jssc.1999.8552, available online at http://www.idealibrary.com on IDEAL®

# Distribution of the Pb and Sb Atoms in the (Pb, Sb)S Layers of the Franckeite-Type Misfit Compound $[(Pb, Sb)S]_{2.28}NbS_2$ Examined by Scanning Tunneling and Atomic Force Microscopy

H. Bengel,* S. Jobic,* Y. Moëlo,* A. Lafond,* J. Rouxel,*,† D.-K. Seo,‡ and M.-H. Whangbo‡

*Institut des Matériaux de Nantes, Laboratoire de Chimie des Solides, UMR CNRS-Université de Nantes 6502, 2 rue de la Houssinière, B.P. 32229, 44322 Nantes Cedex 03, France; ‡Department of Chemistry, North Carolina State University, Raleigh, North Carolina 27695-8204

Received August 3, 1999; in revised form October 12, 1999; accepted October 22, 1999

**The distribution of the Pb and Sb atoms in the (Pb, Sb)S layers of the misfit compound $[(Pb, Sb)S]_{2.28}NbS_2$ was investigated by scanning tunneling microscopy (STM) and atomic force microscopy (AFM). This compound has NaCl-type *MS* (*M* = Pb, Sb) layers (Q-layers) alternating with $NbS_2$ layers (H-layers) in which the Nb atoms are located in slightly distorted trigonal prism sites. Both the H- and Q-layers of $[(Pb, Sb)S]_{2.28}NbS_2$ were imaged by STM and AFM. The atomic-scale STM and AFM images were analyzed in terms of the partial and total electron density plots calculated for the Q- and H-layers. The STM images of the Q-layers allowed us to detect all the constitutive atoms of the Q-layers with a short-range ordering of pure Pb and Sb rows in the $a_Q$ modulation direction.** © 2000 Academic Press

## 1. INTRODUCTION

Several misfit layered chalcogenides (1, 2) exhibit interesting physical properties such as magnetism and superconductivity and hence are interesting compounds for studies concerning how physical properties are affected by low-dimensionality (3). Misfit compounds $(PbS)_{1.14}(NbS_2)_n$ ($n = 1, 2$) have two layers of different periodicity (1–3). Each PbS layer (Q-layer) consists of two NaCl-type PbS sheets, and the Pb atoms in each PbS sheet form distorted square-pyramids with the surrounding S atoms (Fig. 1). The $NbS_2$ layer (H-layer) has a sheet of Nb atoms sandwiched between two sheets of S atoms, and each Nb atom forms an $NbS_6$ trigonal prism as in 2H–$NbS_2$ (Fig. 2). The structure of such a misfit compound is described based on a single-crystal X-ray diffraction analysis using a four-dimensional superspace group (4). The H- and Q-layers have the same *b* parameters, but the ratio of their *a* parameters $a_Q/a_H$ is irrational ("misfit") (5). From a synthetic viewpoint it is crucial to understand what factors determine the stability of such misfit compounds (1, 6). In the mineral cylindrite $[(Pb, Sb)S]_{1.38}[(Sn, Fe)S_2]$, a natural misfit compound, the $Sb^{3+}$ and $Fe^{2+}$ ions preferentially occupy the $Pb^{2+}$ and $Sn^{4+}$ ion sites, respectively, with the $Sb^{3+}:Fe^{2+}$ ratio close to 2 : 1 (7). This pattern of charge-compensating substitution also occurs in synthetic misfit compounds (6). Thus a charge transfer from the Q- to the H-layers and the concomitant Coulombic interaction between them are important for stabilizing misfit compounds.

When the Pb atoms of the Q-layer are partially substituted with Sb atoms in $(PbS)_{1.14}(NbS_2)_n$, the resulting Pb–Sb–Nb–S phases show 2Q/1H, 1Q/1H, and 1Q/2H stacking sequences of the Q- and H-layers (4–6, 8–10). The 2Q/1H misfit compound $[(Pb, Sb)S]_{2.28}NbS_2$ has the franckeite-type structure (10): two consecutive Q-layers alternate with one H-layer; of the two NaCl-type sheets comprising each Q-layer, only one sheet contains the Sb atoms; the Sb-atom-containing sheets are found at the interface between the two Q-layers. Thus the stacking sequence of sheets in $[(Pb, Sb)S]_{2.28}NbS_2$ is written as [PbS–(Pb, Sb)S][(Pb, Sb)S–PbS][S–Nb–S]. The local bonding requirements around the $Sb^{3+}$ and $Pb^{2+}$ ions are slightly different, so the distribution of the Pb and Sb atoms in the (Pb, Sb)S sheets may possess a short-range local order, though not observed by X-ray techniques (10). To check this point, it is necessary to employ local probe techniques such as scanning tunneling microscopy (STM) and atomic force microscopy (AFM) (11–13). A number of STM studies have examined the effect of chemical substitution at atomic level (14–18), and a recent STM/AFM study of the 1Q/1H phase $[(Pb, Sb)S]_{1.14}NbS_2$ showed the presence of a short-range order in the (Pb, Sb)S sheets of the Q-layer (17). In the present work we carried out STM and AFM measurements of $[(Pb, Sb)S]_{2.28}NbS_2$ to examine the distribution of the Pb and Sb atoms in the Q-layer. Atomic-scale STM and AFM images of a layered compound are well described by the partial and total electron density plots [$\rho(r_0, E_F)$ and $\rho(r_0)$, respectively] calculated for its layer (13d, 19, 20), respectively. For a variety of layered materials, the density plots

† Deceased.



0022-4596/00 $35.00

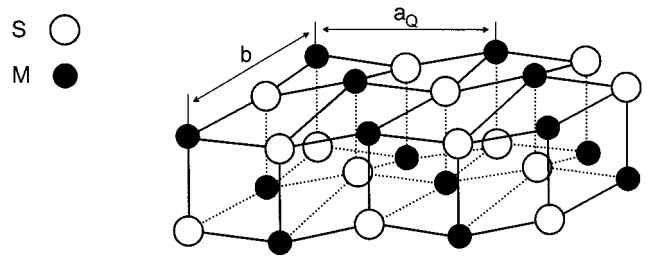


**FIG. 1.** Schematic view of the surface of the Q-layer in $[(Pb, Sb)S]_{2.28}NbS_2$ (adapted from Ref. (2)).

calculated by using the extended Hückel tight binding (EHTB) electronic band structure method (21) were indispensable in interpreting the STM and AFM images (13d). In the present work, the observed STM and AFM images of $[(Pb, Sb)S]_{2.28}NbS_2$ were analyzed by calculating the $\rho(r_0, E_F)$ and $\rho(r_0)$ plots for the Q- and H-layers based on the EHTB method as described elsewhere (13d). The atomic parameters employed for EHTB calculations are summarized in Table 1.

**TABLE 1**

**Exponents $\xi_i$ and Valence Shell Ionization Potentials $H_{ii}$ of Slater-Type orbitals $\chi_i$ Used for Extended Hückel Tight-Binding Calculation[a]**

| Atom | $\chi_i$ | $H_{ii}$ (eV) | $\zeta_i$ | $c_1$[b] | $\zeta'_1$ | $c_2$[b] |
|---|---|---|---|---|---|---|
| Nb | 5*s* | − 10.1 | 1.89 | | | |
| Nb | 5*p* | − 6.86 | 1.85 | | | |
| Nb | 4*d* | − 12.1 | 4.08 | 0.6400 | 1.64 | 0.5516 |
| Pb | 6*s* | − 15.7 | 2.35 | 1.0 | | |
| Pb | 6*p* | − 8.00 | 2.06 | 1.0 | | |
| Sb | 5*s* | − 18.8 | 2.323 | 1.0 | | |
| Sb | 5*p* | − 11.7 | 1.999 | 1.0 | | |
| S | 3*s* | − 20.0 | 2.122 | 1.0 | | |
| S | 3*p* | − 13.3 | 1.827 | 1.0 | | |

[a] The $H_{ii}$ are the diagonal matrix elements $\langle\chi_i|H^{eff}|\chi_i\rangle$, where $H^{eff}$ is the effective Hamiltonian. In our calculations of the off-diagonal matrix elements $H_{ij} = \langle\chi_i|H^{eff}|\chi_j\rangle$, the weighted formula was used. See J. Ammeter, H.-B. Bürgi, J. Thibeault, and R. Hoffmann, *J. Am. Chem. Soc.* **100,** 3686 (1978).

[b] Contraction coefficients used in the double-zeta Slater-type orbital.

## 2. EXPERIMENTAL

The general synthesis conditions for $[(Pb, Sb)S]_{2.28}NbS_2$ were described elsewhere (5). A single-crystal X-ray diffraction analysis of $[(Pb, Sb)S]_{2.28}NbS_2$ suggests a statistical distribution of the Pb and Sb atoms in the (Pb, Sb)S sheets (10). This study solved the structure of the common part and the Q-layer part of $[(Pb, Sb)S]_{2.28}NbS_2$ and showed that the Pb : Sb ratio in the (Pb, Sb)S sheet is close to 3 : 2. The small number of unique reflections did not allow a direct solution for the structure of the H-layer part. The structure of the H-layer part derived from that of the common part shows that the H-layer has the structure 2H–$NbS_2$. The cell parameters of $[(Pb, Sb)S]_{2.28}NbS_2$ are $a_Q = 5.964(2)$ Å, $a_H = 3.33$ Å, $b = 5.8285(9)$ Å, $c = 17.649(6)$ Å, $\alpha = 86.41(2)^\circ$, $\beta = 86.55(3)^\circ$, and $\gamma = 89.97(2)^\circ$. In the structure determination for the Q-layer, the Pb and Sb atoms on the (Pb, Sb)S sheet were constrained to having the same positional parameters, but the relative amount of Pb and Sb for a given site was refined under the condition that the total amount of Pb and Sb at the site is equal to the occupancy of the site. (Thus $x = 0.5608(7)$, $y = 0.084(8)$, and $z = 0.0831(3)$ for the Pb2/Sb2 site, and the site occupancy factors of Pb2 and Sb2 are 0.61(8) and 0.39, respectively. See Table 3 of Ref. (10) for more details.) In reality, however, the Pb atoms should lie slightly higher than the Sb atoms, since the Sb–S bonds are shorter than the Pb–S bonds.

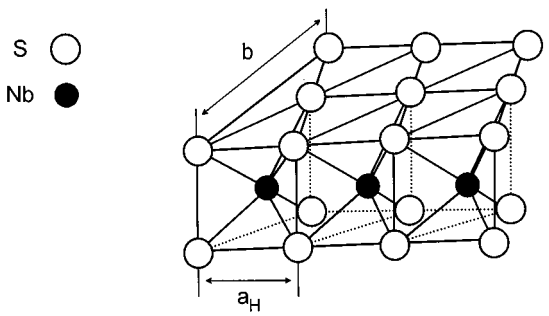


**FIG. 2.** Schematic view of the surface of the H-layer in $[(Pb, Sb)S]_{2.28}NbS_2$ (adapted from Ref. (2)).

STM and AFM images were recorded at ambient conditions with a commercial scanning probe microscope Nanoscope III (Digital Instruments Inc.), equipped with STM and AFM heads. Mechanically sharpened Pt/Ir tips were used for STM, and commercial $Si_3N_4$ tips for AFM. Crystal samples were fixed on a copper support with silver glue and were positioned on stages of both STM and AFM. Measurements were carried out on freshly cleaved surfaces of the crystal samples. Atomic-scale images were recorded in current imaging mode for STM, and in height imaging mode for AFM. To minimize the effects of thermal drift and spontaneous image imperfections associated with possible tip instabilities, a series of images in the "up" and "down" scan directions were collected. Certain images were filtered with the fast Fourier transform procedure to emphasize their periodic features.

In the STM and AFM imaging of $[(Pb, Sb)S]_{2.28}NbS_2$, there are three different atomic surfaces to consider, namely, the S atom sheet of the H-layer as well as the PbS and (Pb, Sb)S sheets of the Q-layer. Which of the three surfaces is imaged under a given experimental condition should depend on the mechanical stability of the Q- and H-layers under the force exerted by the scanning tip. In the STM and

AFM images of layered materials, only the atoms on the surface of the topmost layer can be detected (13d). Thus $\rho(r_0, E_F)$ and $\rho(r_0)$ plots were calculated for isolated Q- and H-layers. Unless otherwise stated, these plots were calculated with the tip placed at 2.0 Å above the most protruded atoms of the surface (i.e., $r_0 = 2.0$ Å). For a homogeneous surface, the essential features of these plots do not depend on $r_0$. For a heterogeneous surface such as the (Pb, Sb)S sheet of the Q-layer, the details of the $\rho(r_0, E_F)$ and $\rho(r_0)$ plots depend on $r_0$ (see below).

## 3. AFM IMAGES

Two types of AFM images are observed for $[(Pb, Sb)S]_{2.28}NbS_2$. In one type, AFM images show a hexagonal pattern of bright spots (Fig. 3). The distance between adjacent bright spots corresponds to the shortest interatomic distance in the S- or Nb-atom sheets of the $NbS_2$-layer. The $\rho(r_0)$ plot calculated for the $NbS_2$ layer (Fig. 4) shows that the bright spots correspond to the surface S atoms. In another type, AFM images have a checkerboard pattern of bright spots (Fig. 5). The distance between adjacent bright spots in Fig. 5 agrees well with the distance between two identical surface atoms, i.e., S-atoms or (Pb, Sb)-atoms, of the Q-layer. Though less frequently, it was possible to record AFM images with a checkerboard pattern in which the center of each square of bright spots contains a less bright spot (Fig. 6).

To simplify our density plot calculations for the Q-layer, we employed a model Q-layer in which the Pb : Sb ratio is 1 : 1 in the (Pb, Sb)S sheet, and the Pb and Sb atoms are arranged in a checkerboard pattern (Fig. 7a). The $\rho(r_0)$ plots calculated for the PbS and (Pb, Sb)S surfaces of this model Q-layer are presented in Figs. 7b and 7c, respectively. The high-electron-density spots are dominated by the Pb atoms in Fig. 7b, and by the Pb and Sb atoms in Fig. 7c. On the pure PbS surface of the Q-layer the Pb atom lies 0.51 Å higher than the S atoms, and on the (Pb, Sb)S surface of the Q-layer the Pb/Sb atoms lie 0.21 Å higher than the S atoms (10). Thus it is not surprising that these $\rho(r_0)$ plots are dominated by the Pb and Sb atoms. Consequently, in Fig. 5 the bright spots with a checkerboard pattern are assigned to the Pb atoms of the PbS sheet or the Pb/Sb atoms of the (Pb, Sb)S sheet in the Q-layer. Likewise, in Fig. 6, the brighter spots are assigned to the Pb/Sb atoms, and the less bright ones to the S atoms.

The $\rho(r_0)$ plot (for $r_0 = 2.0$ Å) of Fig. 7c has a slightly higher density on the Pb than on the Sb atoms. The opposite result is found when $\rho(r_0)$ is calculated for a shorter $r_0$ (e.g., 1.0 Å), because the valence orbitals of Sb are more contracted than those of Pb. However, the former result should be correct because the longer $r_0$ is more realistic and because on the surface of the (Pb, Sb)S sheet the Pb atoms should lie higher than the Sb atoms.

The AFM image of the H-layer in Fig. 3 was captured 52 s before that of the Q-layer in Fig. 5. Thus by comparing Figs. 3 and **5** the orientation of the H-layer relative to the Q-layer can be deduced. The common direction (i.e., *b* direction) is indicated by arrows in both images. The misfit direction is almost perpendicular to the common direction.

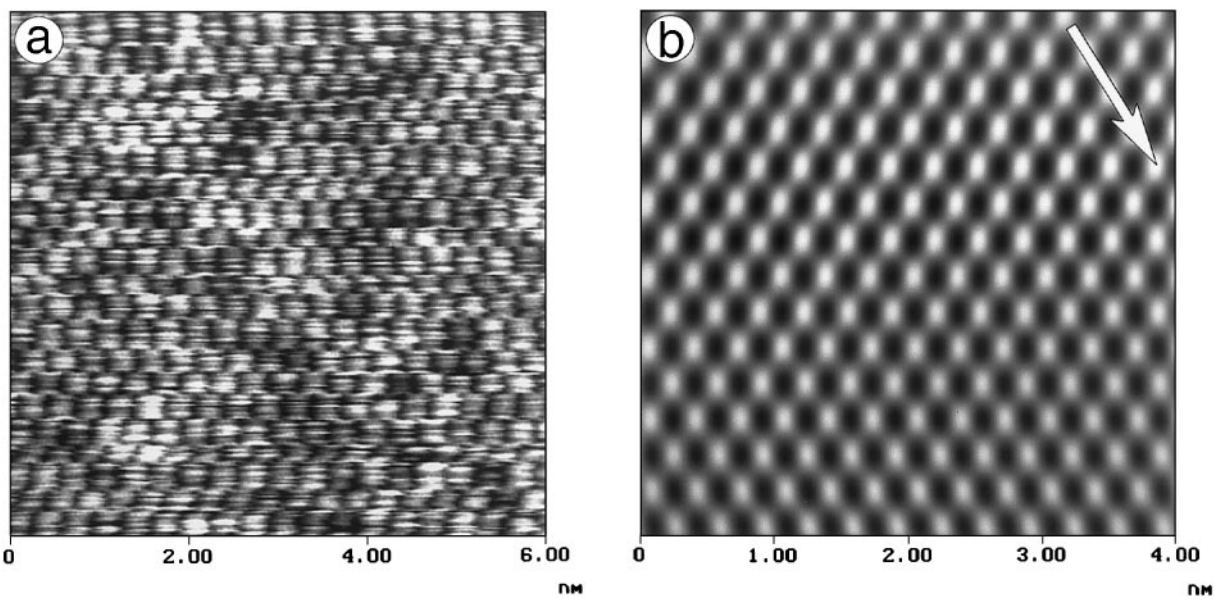


**FIG. 3.** Atomic-scale AFM height images of $[(Pb, Sb)S]_{2.28}NbS_2$: (a) unfiltered image and (b) filtered image of an enlarged part of (a). The contrast covers height variations in the 0.0- to 0.3-nm range, and the arrow in (b) indicates the *b* direction.

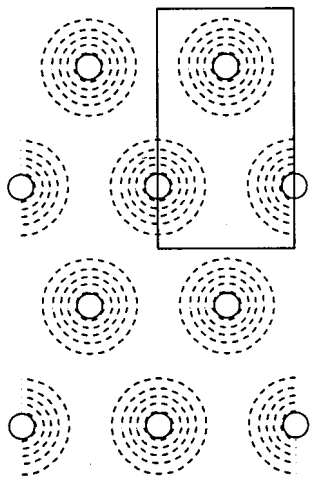

**FIG. 4.** The $\rho(r_0)$ plot calculated for the H-layer of $[(Pb, Sb)S]_{2.28}NbS_2$. Under the simplifying assumption of Pb : Sb = 1 : 1 for the (Pb, Sb)S sheet, the Q-layer has the formula $Pb_3SbS_4^+$. Therefore the formula unit $NbS_2$ of the H-layer has the charge $-1.14$. The contour lines correspond to 0.02, 0.04, 0.06, 0.08, and $0.10 \times 10^{-2}$ electrons/au$^3$. The surface S atoms are represented by circles. The unit cell is indicated by a rectangle.

## 4. STM IMAGES

The STM image of $[(Pb, Sb)S]_{2.28}NbS_2$ in Fig. 8 exhibits a hexagonal pattern of bright spots. The distance between adjacent bright spots is in good agreement with the shortest interatomic distance in the S- or Nb-atom sheet of the H-layer. As shown in Fig. 9 the $\rho(r_0, E_F)$ plot calculated for the H-layer is dominated by the contribution of the surface sulfur atoms. Thus the bright spots of the STM image are associated with the surface S atoms.

Occasionally, it was possible to record STM images that possess no hexagonal pattern of bright spots. In the current mode STM images in Figs. 10a and 10b, "ribbons" consisting of three or two consecutive bright spots are observed. The contrast variation in the "3-spot-ribbons" is much stronger than that in the "2-spot-ribbons." It is important to notice that when the bright and less-bright spots are considered as a whole, the STM image has a checkerboard pattern. These spots show an average periodicity close to the near-square pattern expected for the Q-layer (i.e., 2.98 Å × 2.92 Å). Since the distance between adjacent bright spots corresponds to the nearest neighbor distance on the surface atoms of the Q-layer, the bright spots in the STM images of Figs. 10a and 10b should represent the Pb and S atoms of the pure PbS sheet or the Pb/Sb and S atoms of the (Pb, Sb)S sheet. This conclusion is furthermore confirmed by density plot calculations. The $\rho(r_0, E_F)$ plots calculated for the PbS and (Pb, Sb)S surfaces of the model Q-layer are presented in Figs. 11a and 11b, respectively. These plots are dominated by the Pb atoms. In the $\rho(r_0, E_F)$ plot of the (Pb, Sb)S surface calculated for $r_0 = 1.0$ Å, the Sb atoms have a slightly higher density than do the Pb atoms, and the main contributors of the density are the in-plane p-orbitals of Sb and the out-of-plane *p*-orbital of Pb. (For $r_0 = 0.5$ Å, the S atoms also contribute to the $\rho(r_0, E_F)$ plot.) In our calculations for the (Pb, Sb)S surface, the Pb and Sb

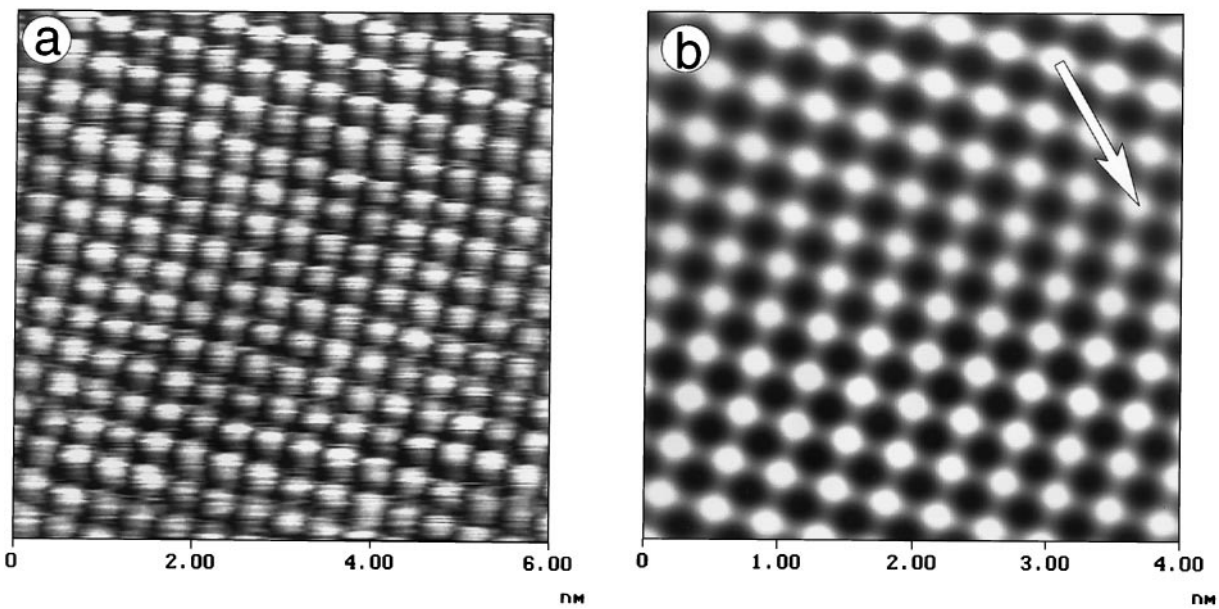


**FIG. 5.** Atomic-scale AFM height images of $[(Pb, Sb)S]_{2.28}NbS_2$: (a) unfiltered image and (b) filtered image of an enlarged part of (a). The contrast covers height variations in the 0.0- to 0.8-nm range, and the arrow in (b) indicates the *b* direction.

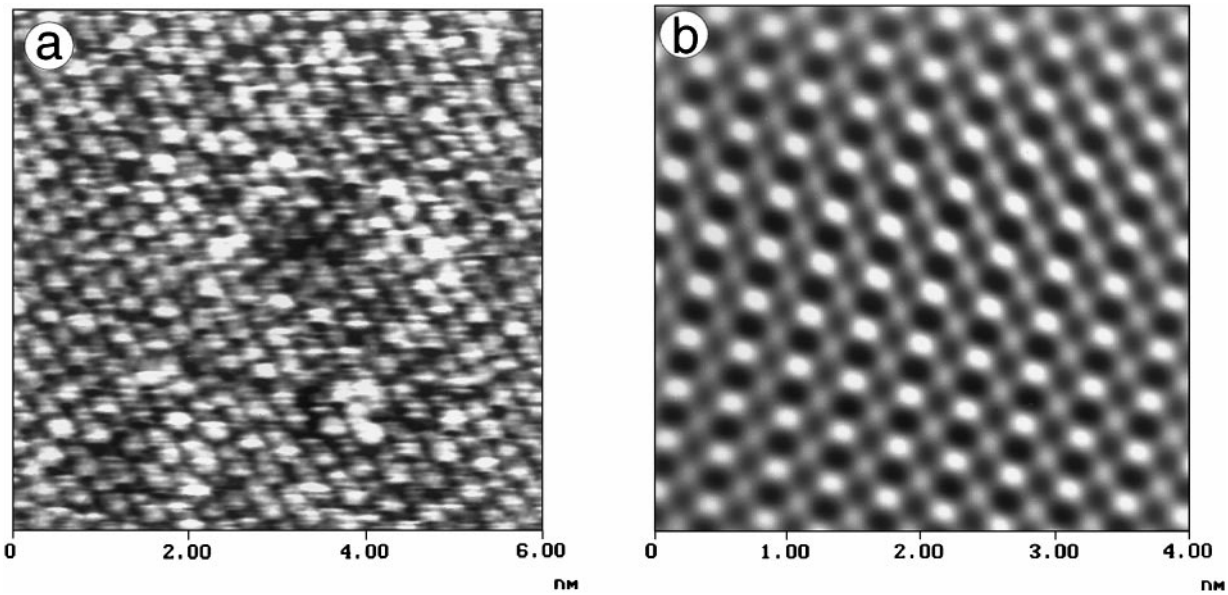


**FIG. 6.** Atomic-scale AFM height images of $[(Pb, Sb)S]_{2.28}NbS_2$: (a) unfiltered image and (b) filtered image of an enlarged part of (a). The contrast covers height variations in the 0.0- to 0.4-nm range.

atoms are considered to have the same height as determined by the X-ray crystal structure determination. However, in reality, the Pb atoms should lie higher than the Sb atoms on the (Pb, Sb)S surface because the Pb–S bonds are longer than the Sb–S bonds. Thus in Figs. 10a and 10b, it is most reasonable to assign the brightest spots to the Pb atoms, the less-bright spots to the Sb atoms, and the darkest spots to the S atoms of the Q-layer. That is, the images of Figs. 10a and 10b correspond to the (Pb, Sb)S surface of the Q-layer.

If the Pb/Sb and S atoms are present as assigned, the bright spots of Fig. 10b should be divided into two widely different square lattices, one representing S atoms and the other representing the Pb/Sb atoms. The images of Figs. 10c and 10d are obtained from Fig. 10b by removing half the bright spots; every second bright spot is suppressed in Fig. 10c, and every other second bright spot in Fig. 10d. Indeed, the images of Figs. 10c and 10d differ strongly in their brightness contrasts: Fig. 10c exhibits a weak contrast variation, while Fig. 10d shows a strong contrast variation.

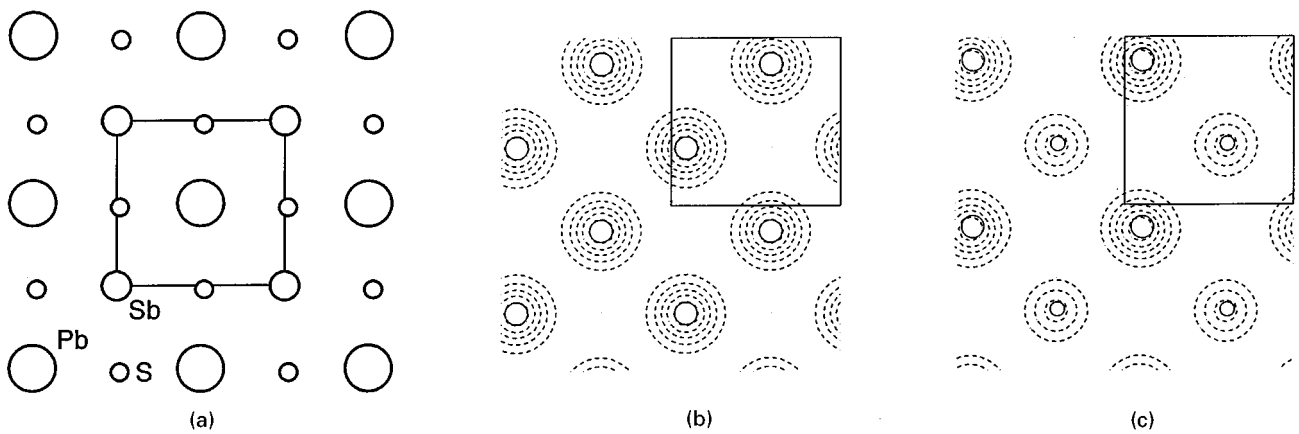


**FIG. 7.** (a) Checkerboard arrangement of Pb and Sb atoms on the (Pb, Sb)S sheet in the Q-layer of $[(Pb, Sb)S]_{2.28}NbS_2$. The large, medium, and small circles represent the surface Pb, Sb, and S atoms, respectively. With the Pb:Sb ratio of 1 : 1, the model Q-layer has the formula unit $Pb_3SbS_4^+$. (b) The $\rho(r_0)$ plot calculated for the PbS surface of the model Q-layer. The contour lines correspond to 0.13, 0.25, 0.37, 0.49, and $0.61 \times 10^{-22}$ electrons/au$^3$. The Pb atoms are represented by circles, and the S atoms are not shown. (c). The $\rho(r_0)$ plot calculated for the (Pb, Sb)S surface of the model Q-layer. The contour lines correspond to 0.14, 0.26, 0.38, 0.50, and $0.63 \times 10^{-12}$ electrons/au$^3$. The surface Pb and Sb atoms are represented by larger and smaller circles, respectively, and the surface S atoms are not shown. The unit cell is indicated by a rectangle.

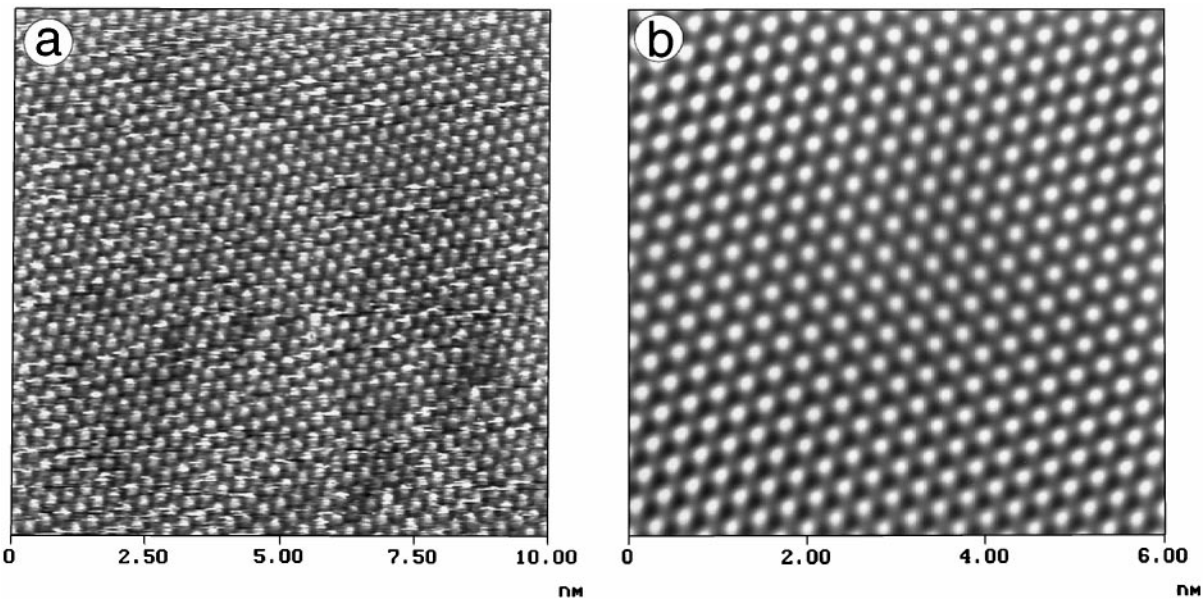


**FIG. 8.** Atomic-scale STM current images of $[(Pb, Sb)S]_{2.28}NbS_2$ ($I_{set} = 4$ nA, $V_{bias} = 77$ mV): (a) unfiltered image and (b) filtered image of an enlarged part of (a). The contrast covers current variations in relative units.

It is most likely that Fig. 10d represents the Pb/Sb atoms. According to electron microprobe and crystal structure analyses (10), the Pb : Sb atom ratio in the (Pb, Sb)S sheet is about 1.50–1.67. Thus if all the Pb and Sb atoms of the (Pb, Sb)S sheet have the same height (which is highly unlikely as stated above), one might expect that its STM image has on average two to three less-bright spots for every three to five bright spots. This point is difficult to prove based on the image of Fig. 10d, because the brightness contrast of the spots varies in a wide range and because the heights of the Pb and Sb atoms on the (Pb, Sb)S sheet cannot be uniform. Nevertheless, it is clear that the STM images of Figs. 10a and 10b represent the (Pb, Sb)S surface of the Q-layer, and that there is a short-range order (along the incommensurate direction $a_Q$) in the distribution of the Pb and Sb atoms as shown in Fig. 10d. In this figure it appears that the brightness modulation along $a_Q$ is due mainly to the succession of pure Pb and Sb mono-atomic rows (parallel to $b$), and also to the height modulation of these rows. Nevertheless, in the studied area of Fig. 10d, there appears a local superstructure $a' = 4a_Q$, in accordance with the simplest commensurate approximation of the interface between the Q and H layers according to the Vernier rule (22): $4a_Q \sim 7a_H$.

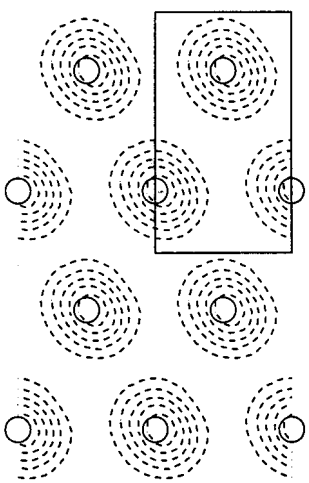

**FIG. 9.** The $\rho(r_0, E_F)$ plot calculated for the H-layer of $[(Pb, Sb)S]_{2.28}NbS_2$. The contour lines correspond to 0.05, 0.10, 0.14, 0.19, and $0.24 \times 10^{-5}$ electrons/au$^3$. The surface S atoms are represented by circles. The unit cell is indicated by a rectangle.

## 5. CONCLUDING REMARKS

For $[(Pb, Sb)S]_{2.28}NbS_2$ the atomic-resolution imaging of the H- and the Q-layers was possible by both STM and AFM. Both STM and AFM images of the H-layer show a hexagonal pattern of bright spots corresponding to the surface S atoms. The AFM images of the Q-layer show a checkerboard pattern of bright spots, which correspond to the Pb atoms of the PbS sheet or the Pb/Sb atoms of the (Pb, Sb)S sheet. The brightness of this pattern is nearly uniform, probably because in the $\rho(r_0)$ plot the Pb and Sb atoms on the (Pb, Sb)S sheet are similar and because the tip–sample contact area is large in AFM (13d). This causes an averaging of small linear patterns, thereby leading to a checkered pattern. The STM images of the Q-layer also exhibit a checkerboard pattern, but this pattern is made up of spots with varying brightness. These STM images are

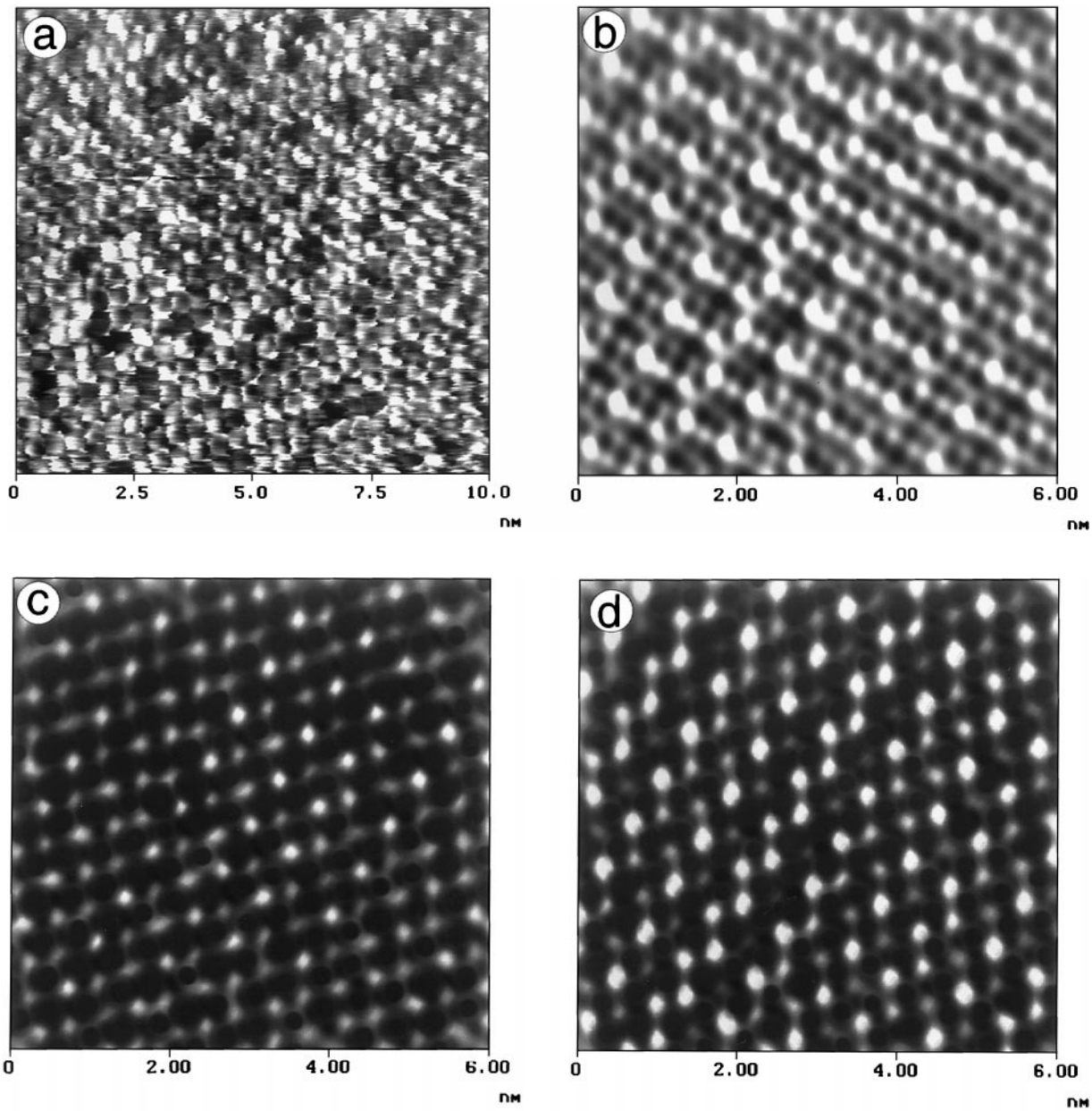


**FIG. 10.** Atomic-scale STM current images of $[(Pb, Sb)S]_{2.28}NbS_2$ ($I_{set} = 14$ nA, $V_{bias} = 11$ mV): (a) unfiltered image and (b) filtered image of an enlarged part of (a). (c, d) Images obtained from the filtered image of (b) by deleting half the bright spots. The contrast covers current variations in relative units.

consistent with the (Pb, Sb)S surface of the Q-layer and indicate that the distribution of the Pb and Sb atoms has a short-range order apparently corresponding to the succession of pure Pb and Sb rows along $a_Q$.

It is important to consider why it is difficult to record STM images of the PbS surface. The $\rho(r_0, E_F)$ plots of Fig. 11 show that the high-electron-density spots of the (Pb, Sb)S surface are stronger than those of the PbS surface by a factor of 10. That is, the (Pb, Sb)S surface should have a greater electrical conductivity than the PbS surface so that under an identical set of tunneling parameters, the tip–sample distance must become shorter on the PbS than on the (Pb, Sb)S surface. Consequently, it is likely that the Q-layer is destroyed during scanning when its PbS surface is exposed to the tip.

Despite the technical constraints, STM/AFM studies of a franckeite-type misfit allowed us to detect the chemical modulation in the Q-layer at the atomic scale. As pointed out first for cylindrite [7], a short-range ordering of atoms with different oxidation states ($Pb^{2+}$ and $Sb^{3+}$) controls the

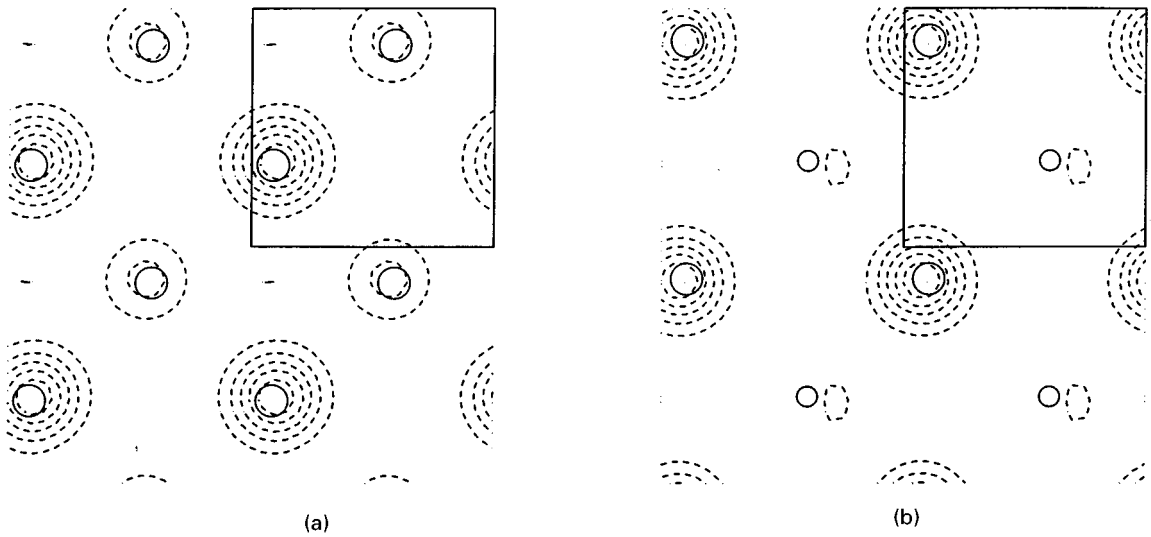


**FIG. 11.** (a) The $\rho(r_0, E_F)$ plot calculated for the PbS surface of the model Q-layer. The contour lines correspond to 0.03, 0.06, 0.09, 0.12, and $0.15 \times 10^{-4}$ electrons/au$^3$. The circles represent the Pb atoms. (b) The $\rho(r_0, E_F)$ plot calculated for the (Pb, Sb)S surface of the model Q-layer. The contour lines correspond to 0.03, 0.06, 0.10, 0.13, and $0.16 \times 10^{-3}$ electrons/au$^3$. The large and small circles represent the Pb and Sb atoms, respectively. In (a) and (b) the rectangle represents a unit cell.

modulation of the charge transfer from the Q- to the H-layer. STM and AFM are useful techniques for deciphering local chemical ordering in misfits, which may play a decisive role in controlling their physical properties (e.g., superconductivity, magnetism, metal/semiconductor transition).

## ACKNOWLEDGMENTS

The work at North Carolina State University was supported by the Office of Basic Energy Sciences, Division of Materials Sciences, U.S. Department of Energy, under Grant DE-FG05-86ER45259. H.B. thanks la Région des Pays de la Loire for the financial support (Grant 185757F).

## REFERENCES

1. G. A. Wiegers and A. Meerschaut, *Mater. Sci. Forum* **100/101,** 101 (1992).
2. G. A. Wiegers and A. Meerschaut, *J. Alloys Comp.* **178,** 351 (1992).
3. J. Rouxel and A. Meerschaut, *Mol. Cryst. Liq. Cryst.* **244,** 343 (1994).
4. G. A. Wiegers, A. Meetsma, R. J. Haange, S. van Smaalen, J. L. de Boer, A. Meerschaut, P. Rabu, and J. Rouxel, *Acta Crystalogr.* **B46,** 324 (1990).
5. A. Lafond, A. Meerschaut, Y. Moëlo, and J. Rouxel, *C.R. Acad. Sci. Paris.* **322,** 165 (1996).
6. Y. Moëlo, A. Meerschaut, J. Rouxel, and C. Auriel, *Chem. Mater.* **7,** 1759 (1995).
7. E. Makovicky, *N. Jb. Miner. Mh. H* **6,** 235 (1974).
8. C. Auriel, A. Meerschaut, and J. Rouxel, *Mater. Res. Bull.* **28,** 675 (1993).
9. J. P. Espinós, A. R. González-Elipe, J. C. Jumas, J. Olivier-Fourcade, J. Morales, J. L. Tirado, and P. Lavela, *Chem. Mater.* **9,** 1393 (1997).
10. A. Lafond, A. Nader, Y. Moëlo, A. Meerschaut, A. Briggs, S. Perrin, P. Monceau, and J. Rouxel, *J. Alloys Compd.* **261,** 114 (1997).
11. G. Binnig, H. Rohrer, Ch. Gerber, and E. Weibel, *Phys. Rev. Lett.* **49,** 57 (1982).
12. G. Binnig, C. F. Quate, and Ch. Gerber, *Phys. Rev. Lett.* **56,** 930 (1986).
13. For reviews, see: (a) R. Wiesendanger and H.-J. Güntherodt, Eds., "Scanning Tunneling Microscopy I, II, and III." Springer Verlag, Heidelberg, 1992, 1993; (b) C. J. Chen, "Introduction to Scanning Tunneling Microscopy." Princeton University Press, Princeton, NJ, 1993. (c) D. A. Bonnell, Ed., "Scanning Tunneling Microscopy and Spectroscopy," VCH, New York, 1993. (d) S. N. Magonov and M.-H. Whangbo, "Surface Analysis with STM and AFM," VCH, Weinheim, 1996.
14. B. A. Parkinson, *J. Am. Chem. Soc.* **112,** 1030 (1990).
15. H. Dai and C. M. Lieber, *J. Chem. Phys.* **97,** 2362 (1993).
16. H. Hillebrecht, P. J. Schmidt, H. W. Rotter, G. Thiele, P. Zönnchen, H. Bengel, H.-J. Cantow, S. N. Magonov, and M.-H. Whangbo, *J. Alloys Compd.* **246,** 70 (1997).
17. H. Bengel, S. Jobic, C. Deudon, J. Rouxel, D.-K. Seo, and M.-H. Whangbo, *Surf. Sci.* **400,** 266 (1998).
18. P. J. Schmidt, G. Thiele, H.-J. Cantow, J. Ren, and M.-H. Whangbo, *J. Phys. Chem. B* **103,** 3626 (1999).
19. J. Tersoff and J. R. Hamman, *Phys. Rev. B* **31,** 805 (1985).
20. B. A. Parkinson, J. Ren, and M.-H. Whangbo, *J. Am. Chem. Soc.* **113,** 7833 (1991).
21. M.-H. Whangbo and R. Hoffmann, *J. Am. Chem. Soc.* **100,** 6093 (1978).
22. E. Makovicky and B. G. Hyde, *Mater. Sci. Forum* **100/101,** 1 (1992).